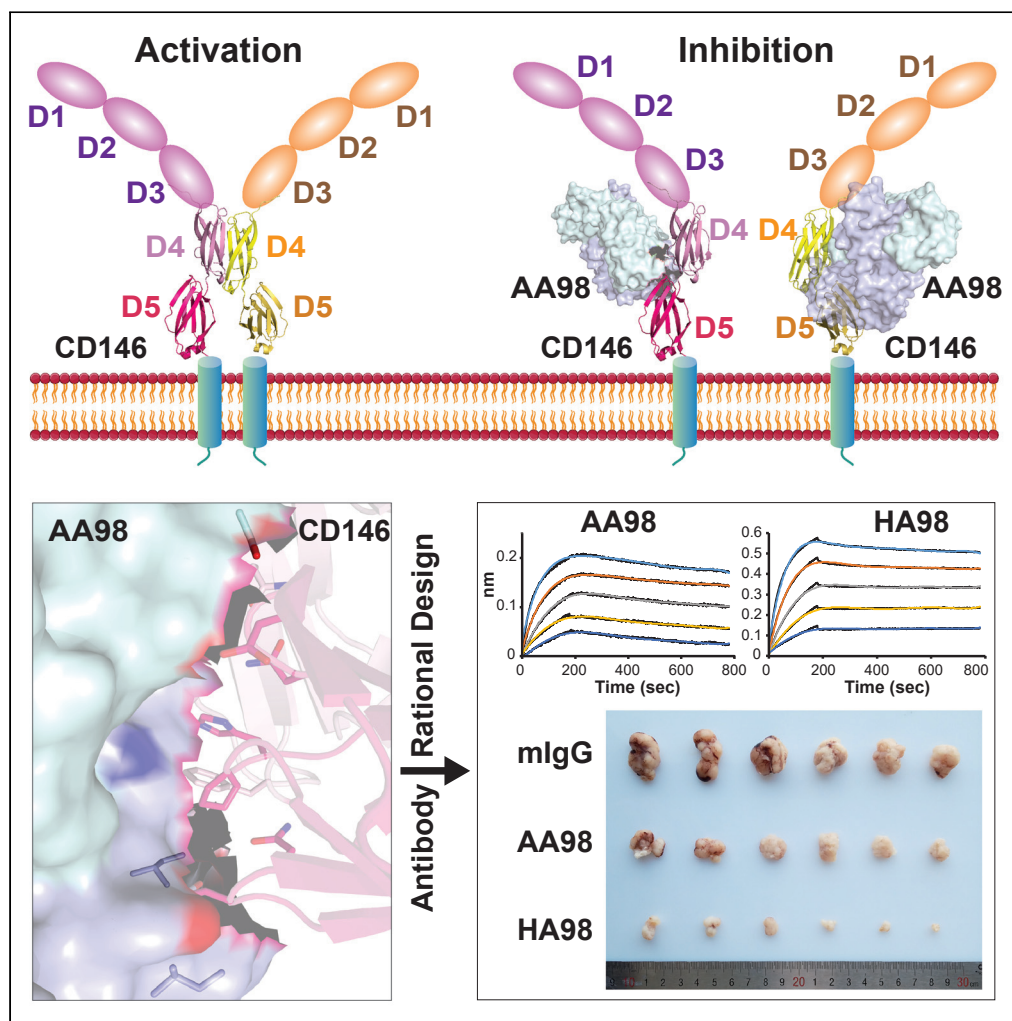


Article

Structure basis for AA98 inhibition on the activation of endothelial cells mediated by CD146



Xuehui Chen,
Huiwen Yan, Dan
Liu, ..., Jing Feng,
Xiyun Yan, Can Xie

fengjing@ibp.ac.cn (J.F.)
yanxy@ibp.ac.cn (X.Y.)
canxie@hmf.ac.cn (C.X.)

Highlights

Structural analysis
elucidated how mAb
AA98 inhibited CD146-
mediated EC activation

AA98-stabilized CD146 in
monomer thus inhibited
activation of EC

Higher affinity monoclonal
antibody HA98 was
rationally designed for
cancer treatment



Article

Structure basis for AA98 inhibition on the activation of endothelial cells mediated by CD146

Xuehui Chen,^{1,2,7} Huiwen Yan,^{3,7} Dan Liu,¹ Qingji Xu,^{1,4} Hongxia Duan,¹ Jing Feng,^{1,*} Xiyun Yan,^{1,4,*} and Can Xie^{2,5,6,8,*}

SUMMARY

CD146 is an adhesion molecule that plays important roles in angiogenesis, cancer metastasis, and immune response. It exists as a monomer or dimer on the cell surface. AA98 is a monoclonal antibody that binds to CD146, which abrogates the activation of CD146-mediated signaling pathways and shows inhibitory effects on tumor growth. However, how AA98 inhibits the function of CD146 remains unclear. Here, we describe a crystal structure of the CD146/AA98 Fab complex at a resolution of 2.8 Å. Monomeric CD146 is stabilized by AA98 Fab binding to the junction region of CD146 domains 4 and 5. A higher-affinity AA98 variant (here named HA98) was thus rationally designed. Better binding to CD146 and prominent inhibition on cell migration were achieved with HA98. Further experiments on xenografted melanoma in mice with HA98 revealed superior inhibitory effects on tumor growth to those of AA98, which suggested future applications of this antibody in cancer therapy.

INTRODUCTION

CD146 is an adhesion molecule (cell adhesion molecule [CAM]) that belongs to the immunoglobulin superfamily (IgSF; Lehmann et al., 1987). It was originally reported as a marker indicating the metastasis of melanoma in 1987. Factors that induce CD146 expression include osmotic pressure, high glucose (Wang et al., 2008), high Ca²⁺ concentration (Schön et al., 2005), and increased cyclic adenosine monophosphate (Rummel et al., 1996). Some growth factors, such as endothelin-1 (Mangahas et al., 2004), transforming growth factor β (Nakai et al., 2016), and nerve growth factor (Taira et al., 2005), enhance the expression of CD146 in melanocytes. Recent studies show that there is a broad and high expression profile of CD146 in embryonic tissues, in contrast to its restricted expression in limited adult normal tissues, such as neovasculature, hair follicular cells, activated T cells, and the intermediate trophoblast (Shih, 1999; Ye et al., 2013). The strict expression control of CD146 in normal adult cells plays a major role in CD146-mediated responses in initiating corresponding reactions (Luca et al., 1993) involved in multiple biological processes, such as reproduction, development, differentiation, and immune response (Wang and Yan, 2013).

More and more literature reported the upregulated expression and pathological functions of CD146 in a variety of carcinomas (Wragg et al., 2016; An et al., 2020; Wang et al., 2015), autoimmune diseases (Dagur and McCoy, 2015), and inflammation-related diseases (Stevenson et al., 2017; Berman et al., 2016). Moreover, CD146 was found to be highly expressed in endothelial cells (ECs) of tumor neovasculature during tumor angiogenesis (Johnson et al., 1996). The pathological upregulation of CD146 was found to promote tumor angiogenesis (Yan et al., 2003), cancer metastasis (Lehmann et al., 1987), and inflammation (Guezuez et al., 2007). Further studies on the mechanisms showed that CD146 mediated the activation of a variety of signaling pathways involved in cell proliferation, migration, viability, motility, and metabolism, such as inhibitor of nuclear factor-kappa B (NF-κB) kinase (Bu et al., 2006), Janus kinase-signal transducer and activator of transcription (Ma et al., 2018), nuclear factor of activated T-cells (Gao et al., 2017), phosphatidylinositol 3-kinase/protein kinase B (Li et al., 2003; Tripathi et al., 2017), Wnt/planar cell polarity (Ye et al., 2013), and mitogen-activated protein kinases (Ma et al., 2018; Chen et al., 2018), when triggered by various ligands. An increasing list of ligands of CD146 including galectin-1, galectin-3, galectin-9 (Colomb et al., 2017; Duan et al., 2020; Jouve et al., 2013), S100A8/A9 (Ruma et al., 2016), Wnt-1, Wnt-5a, Wnt-16 (Zhang et al., 2018; Ye et al., 2013; Tong et al., 2019), fibroblast growth factor 4 (Gao et al., 2017),

¹Key Laboratory of Protein and Peptide Pharmaceuticals, Institute of Biophysics, Chinese Academy of Sciences, Beijing 100101, China

²State Key Laboratory of Membrane Biology, Laboratory of Molecular Biophysics, School of Life Sciences, Peking University, Beijing 100871, China

³Key Laboratory of RNA Biology, Institute of Biophysics, Chinese Academy of Sciences, Beijing 100101, China

⁴College of Life Sciences, University of Chinese Academy of Sciences, Beijing 100049, China

⁵High Magnetic Field Laboratory, Key Laboratory of High Magnetic Field and Ion Beam Physical Biology, Hefei Institutes of Physical Science, Chinese Academy of Sciences, Science Island, Hefei, Anhui 230031, PR China

⁶International Magnetobiology Frontier Research Center, Science Island, Hefei 230031, China

⁷These authors contributed equally

⁸Lead contact

*Correspondence: fengjing@ibp.ac.cn (J.F.), yanxy@ibp.ac.cn (X.Y.), canxie@hmf.ac.cn (C.X.)

<https://doi.org/10.1016/j.isci.2021.102417>



Netrin-1 (Tu et al., 2015), vascular endothelial growth factor C (Yan et al., 2017), as well as extracellular matrix molecules, such as Laminin-411 and Laminin-421 (Ishikawa et al., 2014), suggesting CD146 plays its pathological functions as a receptor, more than just an adhesion molecule.

The CD146 protein is conserved among various species. Mature CD146 protein is a type I receptor that contains five extracellular IgSF domains, a single hydrophobic transmembrane domain, and a short cytoplasmic tail (Lehmann et al., 1987, 1989). The monomeric and dimeric forms of CD146 coexist on the cell surface (Bu et al., 2007). Some of the ligands of CD146, for instance, Netrin-1 could increase the dimeric/monomeric ratio of CD146 (Tu et al., 2015). It was reported that the activation of CD146-mediated signaling depends on its dimerization. The dimeric form of the CD146 cytoplasmic tail could interact with the ezrin-radixin-moesin (actin-linking) proteins and recruit ezrin-radixin-moesin proteins to cell protrusions, promoting the formation and elongation of microvilli (Luo et al., 2012). CD146 promotes tumor angiogenesis through interacting with vascular endothelial growth factor receptor 2 and is thus a component of the vascular endothelial growth factor signalsome (Jiang et al., 2012; Zhuang et al., 2010). CD146 is regarded as a biomarker of malignant metastasis or tumor angiogenesis (Johnson et al., 1996).

AA98, a monoclonal antibody (mAb) that specifically binds to D4-D5 of CD146, suppressed the dimerization of CD146 and abrogated tumor angiogenesis (Zheng et al., 2009), and this inhibitory effect has been confirmed in several *in vivo* xenografted cancers, including melanoma, ovarian cancer, colorectal cancer, hepatocarcinoma, and pancreatic cancer (Jiang et al., 2012; Ma et al., 2017; Xing et al., 2014; Yan et al., 2003), leading to the consideration of AA98 as a potential drug for tumor treatment. The crystal structure of CD146 D4-D5 in complex with AA98 Fab was determined to elucidate the binding interface between AA98 and CD146. Structural rearrangement during monomer-dimer transition was proposed through a structural comparison with other IgSF proteins, and validated with mutagenesis studies. Several mAbs with higher affinity to CD146 based on AA98 were then rationally designed directed by the structural information, which showed higher inhibitory effects on tumor growth, providing optimized candidate for clinical applications targeting CD146.

RESULTS

AA98 Fab binds to the upper region of CD146 domain 5

The mAb AA98 was obtained from the hybridoma generated from the mouse immunized with human umbilical vein endothelial cells (HUVECs). To determine the crystal structure of the CD146 complex with AA98, a human CD146 fragment containing domain 4 and domain 5 (D4-D5 fragment containing residues from Gln336 to Leu519) was expressed in CHO Lec 3.2.8.1 cells and purified to homogeneity. Gel filtration of CD146 D4-D5 showed that the D4-D5 fragment appears to be at single peak in solution with a molecular weight of ~50 kDa, corresponding to the dimer (Figure S1, green curve). The AA98 antibody was purified with a Protein A column, and Fab was generated by papain cleavage (Figure S1, red curve). The CD146 and Fab were mixed at a 1:4 molar ratio, and the complex was further purified with gel filtration to remove excess Fab portions before crystallization (Figure S1, blue curve). X-ray diffraction data were collected to a resolution of 2.8 Å (Table 1), and the structure was solved by molecular replacement using a search model derived from the structure of D2.3 (Protein Data Bank [PDB]: 1YEC; 90% sequence identity to AA98 Fab) (Charbonnier et al., 1997). The structure of CD146 D4-D5 was later obtained from manual model building (Table 1). The crystal accommodates two CD146-Fab complexes in the asymmetric unit of P2₁.

AA98 Fab possessed the typical immunoglobulin fold found in all antibodies, wherein the light chain and heavy chain form the variable domains that bind to the linker region of CD146 D4 and D5 (Figure 1A). The buried surface between CD146 D4 and D5 is 315 Å², which is comparable to the buried surface area among the majority of IgSF domains.

CD146 appears to be monomeric in the complex structure, and its D4 and D5 are both Ig-like C2-type domains (Figures 1A, S2A, and S2B). A short linker and hydrogen bond network surrounding the CD146 D4-D5 linker region further consolidate the rigidity between two domains (Figures S3A and S3B). The structure shows a sharp bend of ~120° between the successive domains. Two N-glycosylation sites on D4 and D5 were identified in the electron density map (Figure 1A). Both D4 and D5 contain two beta (β) sheets, composed of β strands ABE and GFCC' in D4 and ABED and A'GFC in D5, respectively (Figure 1A). Compared with typical C2-type domains (Wang and Springer, 1998), D5 contains one additional β strand,

Table 1. Data collection and refinement statistics

Data collection	
Beamline	SSRF BL19U
Data collection temperature (K)	100
Wavelength	0.979 Å
Space group	$P2_1$
N subunits/asym unit	2
Unit cell	$a = 84.2 \text{ \AA}; b = 88.4 \text{ \AA}; c = 94.6 \text{ \AA}$ $\alpha = 90^\circ; \beta = 89.9^\circ; \gamma = 90^\circ$
Resolution, Å	29.7–2.8 (2.90–2.8)
Total reflections	30,870/2757
Completeness, %	88.7
R _p im	0.045 (0.453)
CC 1/2	0.93 (0.700)
I/σ (I)	10.4 (7.7)
Redundancy	5.5 (5.3)
Refinement statistics	
Refinement range, Å	29.7–2.8 (2.9–2.8)
Wilson B-factor	64.72
Reflections used in refinement	30,863/2755
Reflections used for R-free	1581 (120)
Average B-factors (Å ²) protein	66.90
R-work	0.217 (0.317)
R-free	0.262 (0.393)

Statistics for the highest-resolution shell are shown in parentheses.

D, which is located at the binding site of AA98 Fab and appears to be flexible compared with the rest of the molecule (Figure 1A).

The superposition of the two most closely related IgSF structures, domains 1 and 2 of human CD166 (PDB: 5A2F; 23% sequence identity (Chappell et al., 2015)) and domains 3 and 4 of DCC (PDB: 3LAF; 25% sequence identity (Chen et al., 2013)), on D4 and D5 of CD146 structure also reveals a distinct bend between CD146 D4 and D5 (Figure 1B). The orientation of D4 relative to its adjacent D5 (120°) is obviously different from the extended conformation prevalently adopted by IgSF proteins between successive domains. This unusual bend (Yang et al., 2004) in the complex structure may possibly be caused by the conformational change after the binding of AA98 Fab (Figure 1A).

Superposition of the two CD146 D4-D5 from the asymmetric unit shows that these two molecules were almost identical (root-mean-square deviation from the superposition of the CD146 Cα atoms is 0.31 Å), even at the interdomain linker (Figure S2C). This may be owing to the AA98 Fab binding and thus fixed the relative position of these two successive domains and the interdomain linker. Apart from this, the unexpected extremely short linker (two residues) between D4 and D5 might also contribute to this rigidity. The diversity of interdomain geometry is crucial for IgSF receptors to interact with multiple ligands. Unfortunately, because of the lack of CD146 structure, we are not clear whether this extremely short linker is natural existence or the cause of the conformational change from the antibody binding.

Mutation studies of the CD146 D4-D5 dimer interface

D4 and D1 in intercellular adhesion molecule 1 (ICAM-1) were suggested as major intramolecular and intermolecular dimerization interfaces, respectively (Yang et al., 2004). Sixteen residues were disordered in the ICAM-1 dimeric D4 structure, which formed part of the BC loop, CE loop, and strand C in the ICAM-1 D4 monomer structure. In dimeric ICAM-1 D4, strands from two D4s form two super sheets. Subsequent

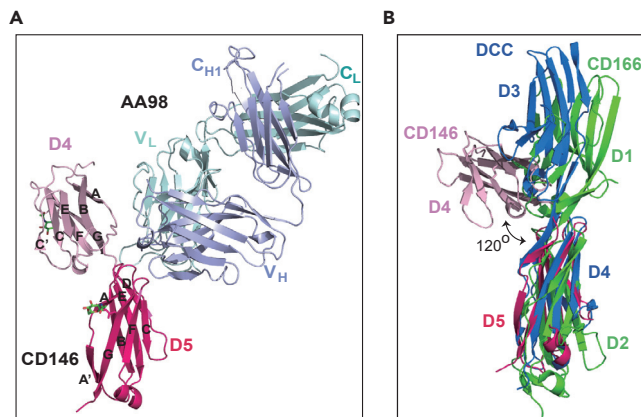


Figure 1. Overall structure of CD146 D4-D5 in complex with AA98 Fab

(A) Ribbon diagrams of CD146 D4-D5 in complex with AA98 Fab. CD146 D4 is shown in light pink, whereas D5 is shown in hot pink. The AA98 Fab light and heavy chains are shown in pale cyan and light blue, respectively. Glycans are drawn in stick representation with red oxygens and green carbons.

(B) Superposition of AA98 Fab-bound CD146 D4-D5 with D1-D2 of CD166 (5A2F) and D3-D4 of DCC (3LAF). The superposition is on CD146 D5. CD146 D4 is shown in light pink, whereas D5 is shown in hot pink. CD166 D1-D2 is shown in green, and DCC D3-D4 is shown in marine. The angle of 120° between the Fab-bound CD146 D4 and D5 is distinctively different from those in CD166 and DCC.

See also [Figures S1–S3](#).

deletions of strand C or strand E in D4 cause a change from the coexistence of monomeric and dimeric forms in wild-type ICAM-1 to dimeric forms in these deletion mutants (Chen et al., 2007). To address whether a similar dimerization mode occurred in the CD146 extracellular region, chemical crosslinking and mass spectrometric analysis of the CD146 D4-D5 homodimer was performed. K398 in D4 and K439 in D5 were then identified as part of the dimerization interface (Figure 2A). In the complex structure of CD146 D4-D5/AA98 Fab, K398 is located in the CE loop of D4, whereas K439 is located in strand A' of D5 (Figures 2A and 2B). Superposition of the CD146 D4-D5 structure with the ICAM-1 dimeric structure (PDB: 1P53) reveals that K398 in CD146 D4 is buried in the dimer interface and K439 on CD146 D5 appears in between two D5 domains and in close contact with corresponding residues from another D5 if a similar dimerization pattern is adopted (Figure 2B), which is in agreement with the cross-linking data and much as in ICAM-1 (Yang et al., 2004).

To validate the dimerization interface, we deleted the C strand (Δ 374E-380E) or the E strand (Δ 390P-396D) and constructed two more deletions (Δ 367A-386L and Δ 387E-399R), which extended the deletion to the adjacent loops in D4 to determine if these residues are involved in the monomeric/dimeric structure transition (Figure S4). We transfected human embryonic kidney 293T cells and HUVECs with these mutants and with a C-terminal myc tag for detection. Western blot analysis showed that all the aforementioned deletions profoundly increased the ratio of CD146 dimer on the cell surface in both 293T cells and HUVECs (Figures 2C and 2D). It is interesting to note that the same β strand (strand C and E) in ICAM-1 is also involved in dimerization (Yang et al., 2004; Chen et al., 2007).

In the complex structure, β strand E is the only edge strand in the monomeric D4-D5 of CD146 (Figure 3A), and Leu-392 and Leu-394 are two inward-pointing residues exposed to solvent forming a hydrophobic patch (Figure 3A). Thus, L392F and L394F were designed to further enhance the hydrophobic patch and stabilize the monomeric structure. Residue W441 on D5 is predicted to form a Pi-Pi interaction between neighboring molecules in the dimeric form; thus, W441A was designed to disrupt this interaction and decrease the stability of CD146 dimerization. Compared with C strand (Δ 374E-380E) or the E strand (Δ 390P-396D) deletion mutants, which favor dimer, monomer steady-state mutants such as L392F, L394F, and W441A showed significantly decreased dimerization on cell surface (Figures 2C and 2D).

The monomeric/dimeric states of CD146 on the cell surface with these dimer-preferred mutants and monomer steady-state mutants were further confirmed by immunoprecipitation with double-tag system and Western blotting as described previously (Zheng et al., 2009). In brief, the 293T cells or the HUVEC cells

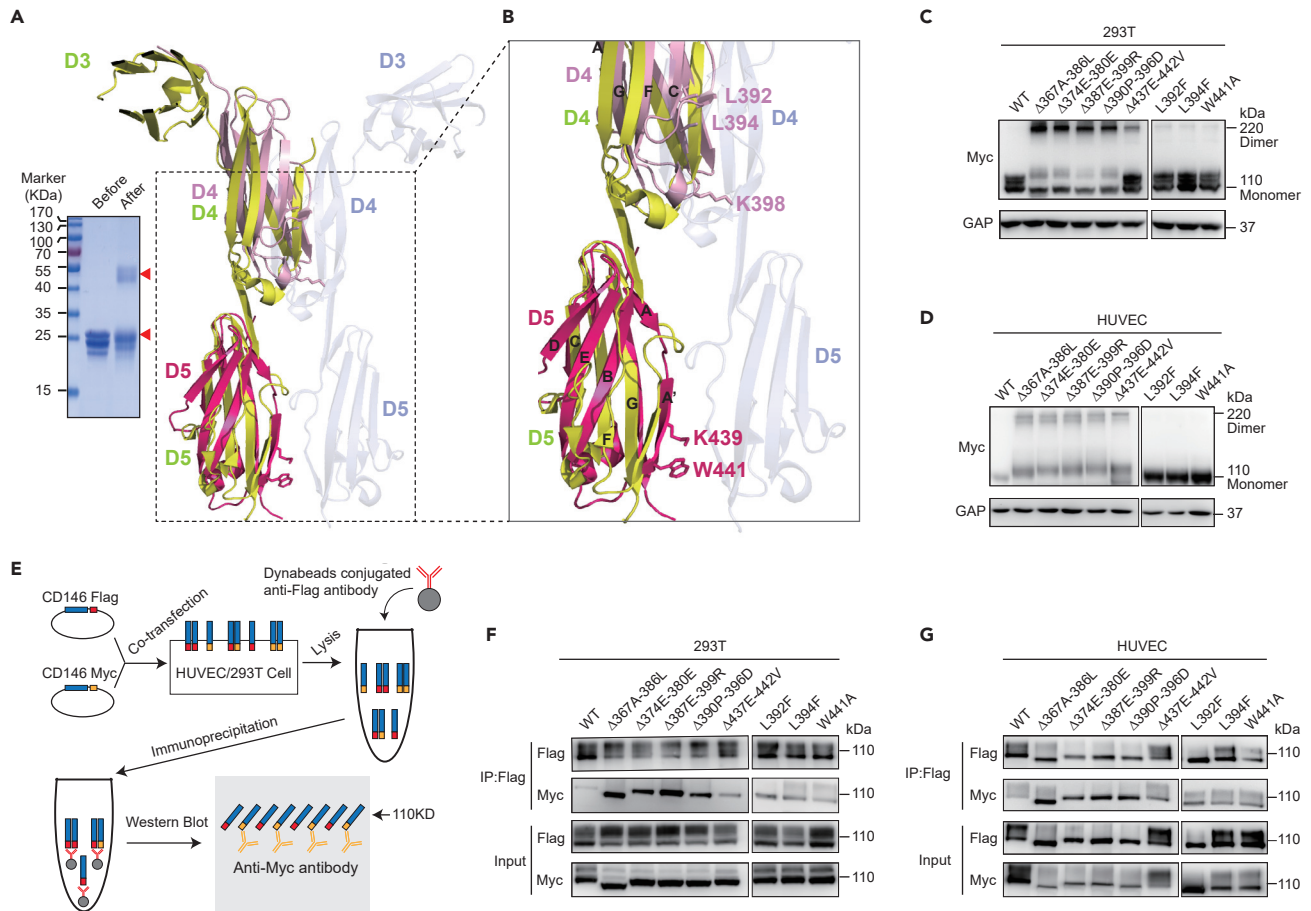


Figure 2. Identification of the potential CD146 dimer interface

(A) Superposition of CD146 D4-D5 on the corresponding domains of the ICAM-1 D3-D5 dimeric form. CD146 D4 is shown in light pink, whereas D5 is shown in hot pink. One monomer of ICAM-1 D3-D5 is shown in yellow, whereas the other is shown in light blue. The two residues, K398 in CD146 D4 and K439 in CD146 D5, that contribute to the dimerization in the chemical cross-linking test shown at the left are drawn in stick representation. Also shown in stick representation are residues that are crucial to the CD146 D4 dimerization, including L392 and L394 in CD146 D4 and W441 in D5. The sodium dodecyl sulphate-polyacrylamide gel electrophoresis (SDS-PAGE) results of chemical crosslinking are shown in the inset (left). Lane before: CD146 D4-D5 protein, Lane after: CD146 D4-D5 mixed with chemical cross-linking reagent BS³ and incubated on ice overnight. A covalently linked CD146 D4-D5 dimer appears in the BS³-treated sample.

(B) Enlargement of the part enclosed with dashed lines in A, showing the residues involved in crosslinking, which are crucial for the D4 dimerization.

(C and D) Western blot analysis of the expression of different mutant constructs in the 293T cell line (C) and in the HUVECs (D).

(E) Cartoon schematic of the double-tag co-immunoprecipitation procedure to identify the existence of CD146 dimer on cell surface.

(F and G) Double-tag co-immunoprecipitation assay analysis of the dimerization of CD146 in the 293T cell line (F) and HUVEC cell line (G). The samples in C and D were run on nonreducing SDS-PAGE, and the samples in F and G were run on reducing SDS-PAGE.

See also [Figure S4](#).

were transfected with full-length CD146 carrying deletion mutants with either an FLAG tag or a Myc tag at C termini simultaneously. CD146 molecules expressed on the cell surface were pulled down by anti-FLAG antibody and then detected either with anti-FLAG mAb or with anti-Myc mAb. Dimeric CD146 molecules with both the affinity tag were detected by the anti-Myc mAb ([Figure 2E](#)). Similar results and conclusions were obtained ([Figures 2F and 2G](#)). The similarity in domain organization and molecular architecture revealed by two IgSF members, CD146 and ICAM-1 ([Figures 2A and 2B](#)), prompted us to speculate whether CD146 D4 employs a similar pattern in dimerization ([Chen et al., 2007](#)).

AA98 depresses EC activation via blocking CD146 dimerization

To explore how the conformational status of CD146 affects the function of ECs, CD146 mutants favoring the dimer or monomer steady state were transfected into HUVECs, and the activation of the HUVECs was

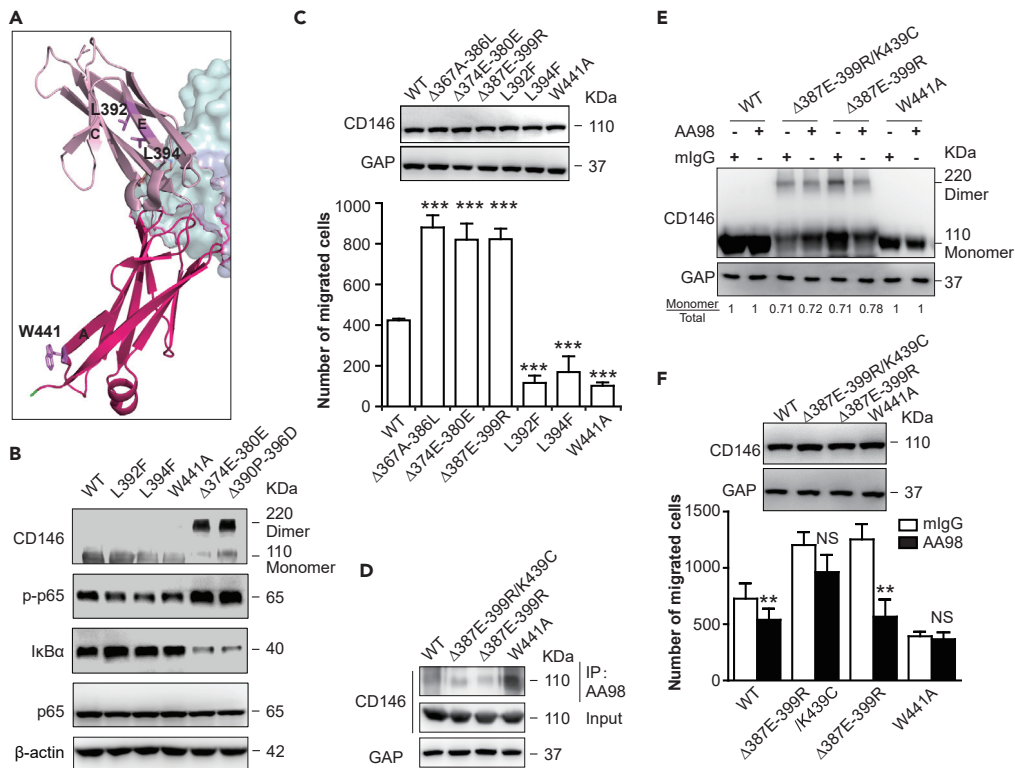


Figure 3. AA98 blocks the dimerization of CD146 to depress EC activation

(A) CD146 D4-D5 in complex with AA98 Fab. CD146 is shown in ribbon representation, D4 is colored in light pink, whereas D5 is colored in hot pink. AA98 Fab is shown in the surface module, and the light and heavy chains are colored in pale cyan and light blue, respectively. Residues L392, L394, and W441, which are crucial for CD146 dimerization, are shown in stick representation.

(B) The activation of NF- κ B signaling caused by the expression of different mutant constructs of CD146 was analyzed by Western blot.

(C) HUVECs transfected with different mutant constructs of CD146 were subjected to a transwell migration assay. Data were represented as mean \pm standard deviation. Significant differences were determined by one-way analysis of variance ($*p < 0.05$; $**p < 0.01$; $***p < 0.001$; ns, no significant difference). Representative images are shown in Figure S7A. Similar expression level of CD146 wild type and mutants was confirmed by Western blot (inset, top).

(D) Co-immunoprecipitation assay analysis of mutant constructs Δ 387E-399R/K439C, Δ 387E-399R, and W441A and of wild-type CD146 expressed in the 293T cell line with AA98.

(E) Western blot analysis of the dimerization of CD146 in mutant-transfected 293T cells treated with AA98 or not.

(F) Transwell assay analysis of the migration activity of mutants transfected with HUVECs treated with AA98 or not. Data were represented as mean \pm standard deviation. Significant differences were determined by one-way analysis of variance ($*p < 0.05$; $**p < 0.01$; $***p < 0.001$; ns, no significant difference). Representative images were shown in Figure S7B. Similar expression level of CD146 wild type and mutants was confirmed by Western blot (inset, top).

See also Figures S5–S7.

tested. As reported in our previous studies, the activation of NF- κ B mediated by CD146 promoted cell migration, while AA98 inhibited cell migration by suppressing NF- κ B signaling mediated by CD146 (Jiang et al., 2012; Bu et al., 2006). The activation of NF- κ B signaling mediated by CD146 mutants was analyzed. Compared with the wild-type CD146, the CD146 mutants with higher dimer ratios (Δ 374E-380E, Δ 390P-396D) promoted the activation of downstream NF- κ B signaling (Figure 3B), the assembly of F-actin (Figure S5), and the migration of ECs (Figure 3C). In contrast, the CD146 mutants that favor steady-state mutants (L392F, L394F, and W441A) inhibited activation of ECs (Figures S5, 3B, and 3C). All these mutations on CD146 do not affect AA98 binding (Figure S6).

We previously reported that AA98 blocks CD146 dimerization on the cell surface, but the blocking mechanism remains to be clarified. The complex structure and the aforementioned mutation studies on the potential dimerization interface between D4 suggested that the AA98 binding interface is distal to and has no

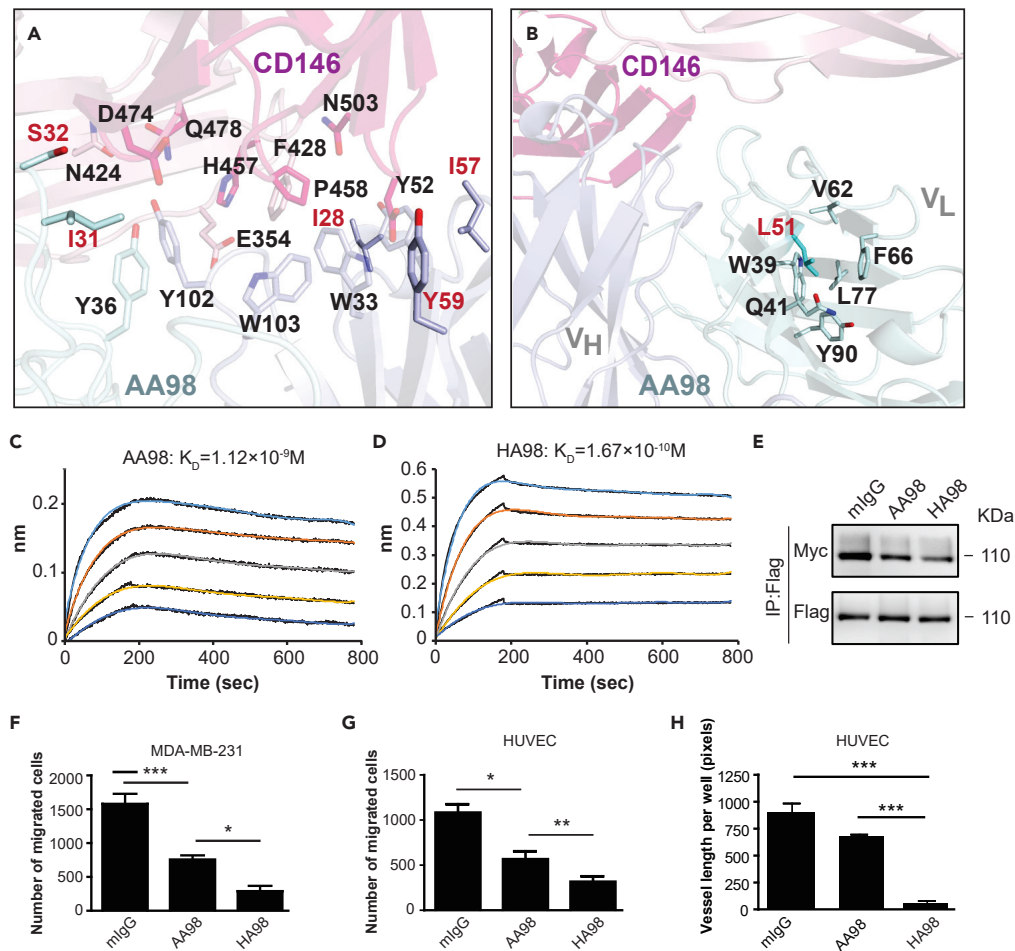
direct influence on the region in D4 involved in CD146 D4 dimerization (Figure 3A). Both the dimeric and monomeric conformations of CD146 can be observed on the cell surface, suggesting a dynamic equilibrium (Bu et al., 2007). It is worth noting that AA98 can bind both dimeric and monomeric forms of CD146 and then stabilize the monomeric form (Zheng et al., 2009). To further validate this hypothesis, a CD146 mutant ($\Delta 387\text{E}-399\text{R}/\text{K}439\text{C}$) was designed with a 387E-399R deletion to increase the dimer ratio and a K439C mutation to stabilize the formed dimer through a disulfide bond (Figure 1D). We transfected HUVECs with this mutant, together with CD146 $\Delta 387\text{E}-399\text{R}$, which favors the dimer; CD146W441A, which favors the monomer; and wild-type CD146, and incubated these cells with AA98 mAb. The AA98 binding of these mutants was confirmed (Figure 3D). As expected, AA98 binding decreased the dimerization ratio in the CD146 $\Delta 387\text{E}-399\text{R}$ mutant but not in the CD146 $\Delta 387\text{E}-399\text{R}/\text{K}439\text{C}$ mutant, in which the dimeric conformation might be locked by disulfide bonds (Figure 3E). Migration experiments further confirmed that AA98 had little inhibitory effect on CD146 $\Delta 387\text{E}-399\text{R}/\text{K}439\text{C}$ mutant (Figure 3F) compared with the significant inhibition in wild-type and CD146 $\Delta 387\text{E}-399\text{R}$ mutant, although the latter also showed increased migration. The disulfide-bond lock abolished AA98 inhibition because of the fixed dimer conformation. The W441A mutant stabilized CD146 in the monomeric form (Figure 3E and 3F) and showed a very low cell migration rate, and the binding of AA98 did not further inhibit the migration rate, suggesting that the monomeric form of CD146 is required for the inhibition. Overall, our results provide further evidence that the AA98 mAb inhibits CD146-promoted cell migration through stabilization of the monomeric form of CD146.

Rational design of AA98 fab with improved affinity and inhibition

The crystal structure of the CD146/AA98 complex provided us with valuable tools to understand the molecular mechanism of the inhibition of CD146-promoted EC activation by AA98. Considering that CD146 is an important pharmaceutical target and that AA98 is currently a potential drug candidate in tumor metastasis and angiogenesis, it is important to redesign the binding interface for improved affinity, which may lead to better inhibition in turn.

The antigen-binding site on AA98 has a shallow concave topology (Figure 4A). The epitope is composed of an aromatic stacking center surrounded by polar interactions. The hydrophobic core is centered on Pro-458 in the BC loop in D5 of CD146. This loop protrudes into the antigen-binding cavity formed by V_H and V_L . The loop, together with aromatic residues, Tyr-102, Trp-103, Trp-33, Tyr-59, and Tyr-52, form the AA98 heavy chain, Tyr-36 form the light chain, His-457 and Pro-458 in D5 and Phe-428 from the D4-D5 linker, forms the major hydrophobic center. The majority of these contacts involve antibody residues from H1, H3, and L1. The heavy-chain hypervariable regions make the most important interactions with CD146, contributing 65% of the buried surface area and most of the polar contacts. The polar interactions surrounding the hydrophobic core involve residues Pro-458, Asp-474, and Gln-478 in D5 and Glu-354 and Asn-424 in D4 (Table 2 and Figure 4A). The AA98 Fab buries 400 \AA^2 of the solvent-accessible surface area on D5 and 290 \AA^2 on D4 at its interface. This result is consistent with the previous report that correct folding of D5 is indispensable for AA98 binding (Zheng et al., 2009).

Humanization is one of the steps required in developing a latent drug for tumor treatment. Unfortunately, the affinity of AA98 for CD146 drops sharply after humanization. How to obtain a higher affinity version of AA98 is the major hurdle to overcome. In the complex structure, residues Ile-28 at the BC loop and Ile-57 and Tyr-59 at the C' strand of the AA98 heavy chain are located near the antigen interface but accessible to the solvent (Figure 4A). We mutated these three residues to acidic or basic residues to strengthen the hydrogen bonds around the hydrophobic center at the interface and stabilize this mAb at the same time. Similar strategies were adopted for residues Ile-31 and Ser-32 in the BC loop of the AA98 light chain. We mutated these two residues to Glu or Thr (Figure 4A). Far from the antigen interface, Leu-51 of the AA98 light chain is an inward-pointing residue constituting the hydrophobic core between the two β sheets in V_L (Figure 4B). We attempted to stabilize this mAb by mutating this residue to Tyr or His. These mutations show increased affinities to the CD146 ectodomain compared with the original AA98 mAb (Table 3 and Figure S8). One of these mutants, I28K/L51Y (here named HA98), binds to endogenous CD146 (Figure S2B) and exhibits heightened affinity to CD146 (Table 3 and Figures 4C and 4D) and better inhibitory effects on dimerization (Figure 4E) and cell migration in both the triple-negative breast cancer cell line MDA-MB-231 (Figure 4F) and HUVECs (Figure 4G). In the tube formation experiment on HUVECs, HA98 also showed a better inhibitory effect than AA98 mAb (Figure 4H). These results not only demonstrated the



success of the rational design of an improved mAb based on structure but also shed light on further application of this antibody in cancer treatment.

HA98 exhibits better inhibition on human melanoma tumor growth

AA98 has been reported previously to inhibit tumor growth by targeting both angiogenesis and tumor cell proliferation (Wang and Yan, 2013; Yan et al., 2003). The optimized version of AA98 that we obtained here, HA98, exhibits higher affinity for the CD146 ectodomain and better inhibition of cell migration and tube

Table 2. Summary of interactions between CD146 D4-D5 and AA98 Fab

CD146	AA98 (H/L)
A351	N57/L
E354	G101/H
Q356	N31/H
N424	Y34/L
F428	W33/H
H457	Y102/H
P458	W33/H
R459	I31/L
D474	I31/L, R96/L
Q475	S32/L
D476	S32/L
Q478	Y102/H
D504	T55/H, R50/H, and W33/H
L505	Y52/H

formation compared with AA98. Our previous result showed that AA98 had an inhibitory effect on the growth of melanoma *in vivo* xenografted mice (Jiang et al., 2012). We repeated this experiment using the human melanoma cell line A375 to compare the effects of AA98 and HA98. Antibody treatment was started when the tumor reached a diameter of 5 to 8 mm, nearly 10 days after xenografts. The growth of human melanoma cells was markedly suppressed by treatment with both AA98 and HA98. A significant reduction in the tumor volume and weight was observed in the HA98 groups compared with both the control groups treated with mIgG and the AA98-treated groups, suggesting that HA98 had a significant inhibitory effect on the growth of melanoma (85%), which was more efficient than that of AA98 (42%; Figures 5A–5C). The body weights of each mouse in the three groups were monitored constantly during the treatment to evaluate the toxicity of HA98. No significant difference in body weight and proliferation of HUVEC was observed among the groups treated with mIgG, AA98, and HA98 (Figures 5D and 5E), which suggests that compared with isotypic IgG and AA98, HA98 had no more significant toxicity. We then detected the vessel intensity in each group by immunochemical staining by anti-CD31. The vessel intensity was much decreased in HA98-treated mice (Figures 5F and 5G). More importantly, the inhibitory effect of HA98 shows little individual variation, which provides a solid foundation for the stability of future treatment.

DISCUSSION

Previous studies have shown that monomeric and dimeric CD146 coexist in equilibrium on the cell surface. The monomeric structure of D4-D5 of CD146 with inhibitory antibody AA98 Fab determined here reveals an unusual bend between the two successive domains compared with other IgSF proteins (Figure 1B), which may be stabilized by AA98 binding. Mutagenesis and chemical cross-linking results indicate that the AA98 binding interface is distal from the dimerization site on D4, and this binding is possible to change the angle between domains and may further push the equilibrium to the monomeric form of CD146.

Parallel (*cis*) interactions are common among CAMs. For example, *cis* dimerization has been demonstrated for CAMs ICAM-1, C-CAM1, and C-CAM2, as well as for N-, E-, and C-cadherins (Miller et al., 1995; Nagar et al., 1996; Brieher et al., 1996; Hunter et al., 1996). It was shown that the dimeric form of C-cadherin is capable of adhesion, whereas the monomeric form is not (Brieher et al., 1996). Our results showed that CD146 mutants in the monomeric state have similar inhibitory effects to those observed on AA98 mAb-bound wild-type CD146 in cell migration, in agreement with previous studies in IgSF.

IgSF is a group of cell surface proteins with characteristic domain organization containing a variable number of Ig-like domains, and various functions have been reported and explored for the members of this superfamily. Similar to ICAM-1, CD146 has five extracellular IgSF domains and equilibrates in the monomer/dimer state on the cell surface through structural rearrangement in D4 and probably in D1 as

Table 3. Affinity of AA98 mAb mutants to CD146 ectodomain

	mAb	K_D value
WT	Wild-type AA98 mAb H/L	1.12×10^{-9}
104–112	Heavy chain (I57E)/light chain (L51Y)	5.07×10^{-10}
104–114	Heavy chain (I57E)/light chain (I31E)	5.36×10^{-10}
H13–111	Heavy chain (I28K)/light chain (L51H)	7.09×10^{-10}
H13–112	Heavy chain (I28K)/light chain (L51Y)	1.67×10^{-10}
H13–115	Heavy chain (I28K)/light chain (I31E/S32T)	6.49×10^{-10}
106–112	Heavy chain (Y59R)/light chain (L51Y)	2.99×10^{-10}
106–114	Heavy chain (Y59R)/light chain (I31E)	2.96×10^{-10}

well (Yang et al., 2004). The dimerization sites are consistent in both molecules, indicating the structural robustness and fundamental stability of the Ig fold in this superfamily.

AA98 was first reported to inhibit the migration and tube formation of ECs *in vitro*. It has also been reported to decrease the growth rates of melanoma, hepatoma, pancreatic, ovarian, and cervical cancer by targeting both angiogenesis and metastasis. Furthermore, AA98 reduces the recruitment of macrophages, which can facilitate the development of tumors. These results show that AA98 inhibits tumor growth and inflammation in different ways. The crystal structure of the CD146/AA98 complex we presented here not only extended our understanding of the inhibition of CD146-promoted EC activation by AA98 but also stimulated the rational design of novel drug candidates. Previous studies have shown an obvious effect of AA98 in tumor inhibition, either independently (Yan et al., 2003; Jiang et al., 2012) or in combination with either antitumor drugs (Ma et al., 2017; Jiang et al., 2012) or radiotherapy (Cheng, 2016). HA98, an optimized version of AA98, shows much better treatment effects, comparable to those in combination therapies. More importantly, the HA98 treatment shows little individual difference, which is an advantage for further exploration for applications as a drug for tumor and inflammation therapy, especially in tumors with high CD146 expression but almost no effective drugs, such as mesenchymal breast cancer and triple-negative breast cancer.

Limitations of the study

Our results show that anti-CD146 mAb AA98 attenuates the activation of CD146-induced promigration signaling pathway via the inhibition of the dimerization of CD146, while the possibility that CD146 functions as monomer is not ruled out.

Resource availability

Lead contact

Further information, requests, and inquiries should be directed to and will be fulfilled by the lead contact, Dr. Can Xie (canxie@hmfl.ac.cn).

Materials availability

This study did not generate new unique reagents.

Data and code availability

The authors declare that all the data supporting the findings of this study are available within the article and its supplemental information files or from the corresponding author upon reasonable request. All the preliminary X-ray structure data are available online in the PDB database (PDB: 6LYN).

METHODS

All methods can be found in the accompanying [transparent methods supplemental file](#).

SUPPLEMENTAL INFORMATION

Supplemental information can be found online at <https://doi.org/10.1016/j.isci.2021.102417>.

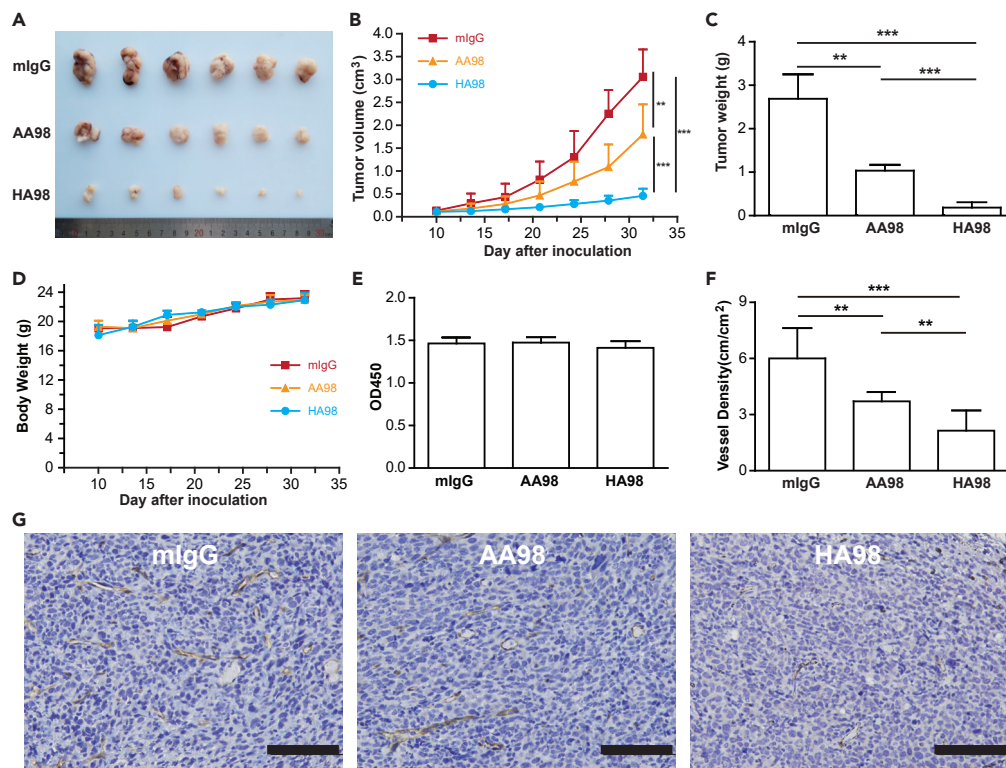


Figure 5. HA98 inhibits tumor growth more efficiently

(A) Representation of human melanoma in xenografted mice.
 (B) Tumor volumes at specific time points after the injection of human melanoma cells A375 (n = 8).
 (C) When the maximal tumor size reached approximately 4 cm³, the mice were killed, and the tumors were excised and weighed.
 (D) Body weight at different time point.
 (E) Proliferation of HUVECs in different treated groups.
 (F) Vessel length in each field of tumors in different groups. Data (B–F) were represented as mean ± standard error. Statistical significance was determined with one-way analysis of variance test (**p < 0.01; ***p < 0.001).
 (G) Immunohistochemical analysis of microvessel density of tumors in different groups. Bars represent 100 μM.

ACKNOWLEDGMENTS

We are grateful to Dr. Sheng Ye from the Institute of Biophysics for helpful discussions regarding crystal structure determination. We thank Yuanyuan Chen, Zhenwei Yang, and Xiaoxia Yu at the Core Facility for Protein Research, Institute of Biophysics, for assistance with experiments. We also thank the Shanghai Synchrotron Radiation Facility for technical support for crystal data collection. This work was supported in part by the grants from the National Natural Science Foundation of China (31770793 to X.C. as well as 31640001 and 31370740 to C.X.), Hefei Institutes of Physical Science, Chinese Academy of Sciences (BJZX201901 to C.X.), and Beijing Municipal Natural Science Foundation, China (7192123 to H.D.).

AUTHOR CONTRIBUTIONS

J.F., X.Y., X.C., and C.X. conceived the idea and designed the study. X.C. performed crystallization and structure determination. X.C. and H.Y. designed and performed tests related to the CD146 D4 dimeric interface and AA98 mutants. Q.X. aided in the aforementioned experiments. D.L. performed the cell migration test. H.D. prepared the AA98 mAb culture supernatant. J.F. contributed to the discussion. X.C., H.Y., X.Y., and C.X. wrote the article. All authors commented on the article.

DECLARATION OF INTERESTS

The authors declare no competing interests.

Received: October 1, 2020

Revised: February 10, 2021

Accepted: April 8, 2021

Published: May 21, 2021

REFERENCES

- An, Y., Wei, N., Cheng, X., Li, Y., Liu, H., Wang, J., Xu, Z., Sun, Z., and Zhang, X. (2020). MCAM abnormal expression and clinical outcome associations are highly cancer dependent as revealed through pan-cancer analysis. *Brief Bioinform.* 21, 709–718.
- Berman, R., Jiang, D., Wu, Q., Stevenson, C.R., Schaefer, N.R., and Chu, H.W. (2016). MUC18 regulates lung rhinovirus infection and inflammation. *PLoS One* 11, e0163927.
- Brieher, W.M., Yap, A.S., and Gumbiner, B.M. (1996). Lateral dimerization is required for the homophilic binding activity of C-cadherin. *J. Cell Biol.* 135, 487–496.
- Bu, P., Gao, L., Zhuang, J., Feng, J., Yang, D., and Yan, X. (2006). Anti-CD146 monoclonal antibody AA98 inhibits angiogenesis via suppression of nuclear factor-kappaB activation. *Mol. Cancer Ther.* 5, 2871–2877.
- Bu, P., Zhuang, J., Feng, J., Yang, D., Shen, X., and Yan, X. (2007). Visualization of CD146 dimerization and its regulation in living cells. *Biochim. Biophys. Acta* 1773, 513–520.
- Chappell, P.E., Garner, L.I., Yan, J., Metcalfe, C., Hatherley, D., Johnson, S., Robinson, C.V., Lea, S.M., and Brown, M.H. (2015). Structures of CD6 and its ligand CD166 give insight into their interaction. *Structure* 23, 1426–1436.
- Charbonnier, J.B., Golinelli-Pimpaneau, B., Gigant, B., Tawfik, D.S., Chap, R., Schindler, D.G., Kim, S.H., Green, B.S., Eshhar, Z., and Knossow, M. (1997). Structural convergence in the active sites of a family of catalytic antibodies. *Science* 275, 1140–1142.
- Chen, J., Luo, Y., Huang, H., Wu, S., Feng, J., Zhang, J., and Yan, X. (2018). CD146 is essential for PDGFR β -induced pericyte recruitment. *Protein Cell* 9, 743–747.
- Chen, Q., Sun, X., Zhou, X.H., Liu, J.H., Wu, J., Zhang, Y., and Wang, J.H. (2013). N-terminal horseshoe conformation of DCC is functionally required for axon guidance and might be shared by other neural receptors. *J. Cell Sci.* 126, 186–195.
- Chen, X., Kim, T.D., Carman, C.V., Mi, L.Z., Song, G., and Springer, T.A. (2007). Structural plasticity in Ig superfamily domain 4 of ICAM-1 mediates cell surface dimerization. *Proc. Natl. Acad. Sci. U S A* 104, 15358–15365.
- Cheng, H. (2016). Inhibiting CD146 by its monoclonal antibody AA98 improves radiosensitivity of cervical cancer cells. *Med. Sci. Monit.* 22, 3328–3333.
- Colomb, F., Wang, W., Simpson, D., Zafar, M., Beynon, R., Rhodes, J.M., and Yu, L.G. (2017). Galectin-3 interacts with the cell-surface glycoprotein CD146 (MCAM, MUC18) and induces secretion of metastasis-promoting cytokines from vascular endothelial cells. *J. Biol. Chem.* 292, 8381–8389.
- Dagur, P.K., and McCoy, J.P., Jr. (2015). Endothelial-binding, proinflammatory T cells identified by MCAM (CD146) expression: characterization and role in human autoimmune diseases. *Autoimmun. Rev.* 14, 415–422.
- Duan, H., Zhao, S., Xiang, J., Ju, C., Chen, X., Gramaglia, I., and Yan, X. (2020). Targeting the CD146/Galectin-9 axis protects the integrity of the blood-brain barrier in experimental cerebral malaria. *Cell Mol. Immunol.* <https://doi.org/10.1038/s41423-020-00582-8>.
- Gao, Q., Zhang, J., Wang, X., Liu, Y., He, R., Liu, X., Wang, F., Feng, J., Yang, D., Wang, Z., et al. (2017). The signalling receptor MCAM coordinates apical-basal polarity and planar cell polarity during morphogenesis. *Nat. Commun.* 8, 15279.
- Guezguez, B., Vigneron, P., Lamerant, N., Kieda, C., Jaffredo, T., and Dunon, D. (2007). Dual role of melanoma cell adhesion molecule (MCAM)/CD146 in lymphocyte endothelium interaction: MCAM/CD146 promotes rolling via microvilli induction in lymphocyte and is an endothelial adhesion receptor. *J. Immunol.* 179, 6673–6685.
- Hunter, I., Sawa, H., Edlund, M., and Obrink, B. (1996). Evidence for regulated dimerization of cell-cell adhesion molecule (C-CAM) in epithelial cells. *Biochem. J.* 320, 847–853.
- Ishikawa, T., Wondimu, Z., Oikawa, Y., Gentilcore, G., Kiessling, R., Egyhazi, B., Hansson, J., and Patarroyo, M. (2014). Laminins 411 and 421 differentially promote tumor cell migration via $\alpha 6 \beta 1$ integrin and MCAM (CD146). *Matrix Biol.* 38, 69–83.
- Jiang, T., Zhuang, J., Duan, H., Luo, Y., Zeng, Q., Fan, K., Yan, H., Lu, D., Ye, Z., Hao, J., et al. (2012). CD146 is a coreceptor for VEGFR-2 in tumor angiogenesis. *Blood* 120, 2330–2339.
- Johnson, J.P., Rummel, M.M., Rothbacher, U., and Sers, C. (1996). MUC18: a cell adhesion molecule with a potential role in tumor growth and tumor cell dissemination. *Curr. Top. Microbiol. Immunol.* 213, 95–105.
- Jouve, N., Despoix, N., Espeli, M., Gauthier, L., Cypowyj, S., Fallague, K., Schiff, C., Dignat-George, F., Vély, F., and Leroyer, A.S. (2013). The involvement of CD146 and its novel ligand Galectin-1 in apoptotic regulation of endothelial cells. *J. Biol. Chem.* 288, 2571–2579.
- Lehmann, J.M., Holzmann, B., Breitbart, E.W., Schmiegelow, P., Riethmüller, G., and Johnson, J.P. (1987). Discrimination between benign and malignant cells of melanocytic lineage by two novel antigens, a glycoprotein with a molecular weight of 113,000 and a protein with a molecular weight of 76,000. *Cancer Res.* 47, 841–845.
- Lehmann, J.M., Riethmüller, G., and Johnson, J.P. (1989). MUC18, a marker of tumor progression in human melanoma, shows sequence similarity to the neural cell adhesion molecules of the immunoglobulin superfamily. *Proc. Natl. Acad. Sci. U S A* 86, 9891–9895.
- Li, G., Kalabis, J., Xu, X., Meier, F., Oka, M., Bogenrieder, T., and Herlyn, M. (2003). Reciprocal regulation of MelCAM and AKT in human melanoma. *Oncogene* 22, 6891–6899.
- Luca, M., Hunt, B., Bucana, C.D., Johnson, J.P., Fidler, I.J., and Bar-Eli, M. (1993). Direct correlation between MUC18 expression and metastatic potential of human melanoma cells. *Melanoma Res.* 3, 35–40.
- Luo, Y., Zheng, C., Zhang, J., Lu, D., Zhuang, J., Xing, S., Feng, J., Yang, D., and Yan, X. (2012). Recognition of CD146 as an ERM-binding protein offers novel mechanisms for melanoma cell migration. *Oncogene* 31, 306–321.
- Ma, X., Wang, J., Liu, J., Mo, Q., Yan, X., Ma, D., and Duan, H. (2017). Targeting CD146 in combination with vorinostat for the treatment of ovarian cancer cells. *Oncol. Lett.* 13, 1681–1687.
- Ma, Y., Zhang, H., Xiong, C., Liu, Z., Xu, Q., Feng, J., Zhang, J., Wang, Z., and Yan, X. (2018). CD146 mediates an E-cadherin-to-N-cadherin switch during TGF- β signaling-induced epithelial-mesenchymal transition. *Cancer Lett.* 430, 201–214.
- Mangahas, C.R., dela Cruz, G.V., Schneider, R.J., and Jamal, S. (2004). Endothelin-1 upregulates MCAM in melanocytes. *J. Invest. Dermatol.* 123, 1135–1139.
- Miller, J., Knorr, R., Ferrone, M., Houdei, R., Carron, C.P., and Dustin, M.L. (1995). Intercellular adhesion molecule-1 dimerization and its consequences for adhesion mediated by lymphocyte function associated-1. *J. Exp. Med.* 182, 1231–1241.
- Nagar, B., Overduin, M., Ikura, M., and Rini, J.M. (1996). Structural basis of calcium-induced E-cadherin rigidification and dimerization. *Nature* 380, 360–364.
- Nakai, T., Sakai, D., Nakamura, Y., Nukaga, T., Grad, S., Li, Z., Alini, M., Chan, D., Masuda, K., Ando, K., et al. (2016). CD146 defines commitment of cultured annulus fibrosus cells to express a contractile phenotype. *J. Orthop. Res.* 34, 1361–1372.
- Ruma, I.M., Putranto, E.W., Kondo, E., Murata, H., Watanabe, M., Huang, P., Kinoshita, R., Futami, J., Inoue, Y., Yamauchi, A., et al. (2016). MCAM, as a novel receptor for S100A8/A9, mediates progression of malignant melanoma through prominent activation of NF- κ B and ROS formation upon ligand binding. *Clin. Exp. Metastasis* 33, 609–627.

- Rummel, M.M., Sers, C., and Johnson, J.P. (1996). Phorbol ester and cyclic AMP-mediated regulation of the melanoma-associated cell adhesion molecule MUC18/MCAM. *Cancer Res.* 56, 2218–2223.
- Schön, M., Kähne, T., Gollnick, H., and Schön, M.P. (2005). Expression of gp130 in tumors and inflammatory disorders of the skin: formal proof of its identity as CD146 (MUC18, Mel-CAM). *J. Invest. Dermatol.* 125, 353–363.
- Shih, I.M. (1999). The role of CD146 (Mel-CAM) in biology and pathology. *J. Pathol.* 189, 4–11.
- Stevenson, C., Jiang, D., Schaefer, N., Ito, Y., Berman, R., Sanchez, A., and Chu, H.W. (2017). MUC18 regulates IL-13-mediated airway inflammatory response. *Inflamm. Res.* 66, 4–11.
- Taira, E., Kohama, K., Tsukamoto, Y., Okumura, S., and Miki, N. (2005). Gicerin/CD146 is involved in neurite extension of NGF-treated PC12 cells. *J. Cell Physiol.* 204, 632–637.
- Tong, W., Zeng, Y., Chow, D.H.K., Yeung, W., Xu, J., Deng, Y., Chen, S., Zhao, H., Zhang, X., Ho, K.K., et al. (2019). Wnt16 attenuates osteoarthritis progression through a PCP/JNK-mTORC1-PTHrP cascade. *Ann. Rheum. Dis.* 78, 551–561.
- Tripathi, S.C., Fahrman, J.F., Celik, M., Aguilar, M., Marini, K.D., Jolly, M.K., Katayama, H., Wang, H., Murage, E.N., Dennison, J.B., et al. (2017). MCAM mediates chemoresistance in small-cell lung cancer via the PI3K/AKT/SOX2 signaling pathway. *Cancer Res.* 77, 4414–4425.
- Tu, T., Zhang, C., Yan, H., Luo, Y., Kong, R., Wen, P., Ye, Z., Chen, J., Feng, J., Liu, F., et al. (2015). CD146 acts as a novel receptor for netrin-1 in promoting angiogenesis and vascular development. *Cell Res.* 25, 275–287.
- Wang, J., and Springer, T.A. (1998). Structural specializations of immunoglobulin superfamily members for adhesion to integrins and viruses. *Immunol. Rev.* 163, 197–205.
- Wang, J., Tang, X., Weng, W., Qiao, Y., Lin, J., Liu, W., Liu, R., Ma, L., Yu, W., Yu, Y., et al. (2015). The membrane protein melanoma cell adhesion molecule (MCAM) is a novel tumor marker that stimulates tumorigenesis in hepatocellular carcinoma. *Oncogene* 34, 5781–5795.
- Wang, N., Fan, Y., Ni, P., Wang, F., Gao, X., Xue, Q., and Tang, L. (2008). High glucose effect on the role of CD146 in human proximal tubular epithelial cells in vitro. *J. Nephrol.* 21, 931–940.
- Wang, Z., and Yan, X. (2013). CD146, a multi-functional molecule beyond adhesion. *Cancer Lett.* 330, 150–162.
- Wragg, J.W., Fingleton, J.P., Anderson, J.A., Ferguson, H.J., Porfiri, E., Bhatt, R.I., Murray, P.G., Heath, V.L., and Bicknell, R. (2016). MCAM and LAMA4 are highly enriched in tumor blood vessels of renal cell carcinoma and predict patient outcome. *Cancer Res.* 76, 2314–2326.
- Xing, S., Luo, Y., Liu, Z., Bu, P., Duan, H., Liu, D., Wang, P., Yang, J., Song, L., Feng, J., et al. (2014). Targeting endothelial CD146 attenuates colitis and prevents colitis-associated carcinogenesis. *Am. J. Pathol.* 184, 1604–1616.
- Yan, H., Zhang, C., Wang, Z., Tu, T., Duan, H., Luo, Y., Feng, J., Liu, F., and Yan, X. (2017). CD146 is required for VEGF-C-induced lymphatic sprouting during lymphangiogenesis. *Sci. Rep.* 7, 7442.
- Yan, X., Lin, Y., Yang, D., Shen, Y., Yuan, M., Zhang, Z., Li, P., Xia, H., Li, L., Luo, D., et al. (2003). A novel anti-CD146 monoclonal antibody, AA98, inhibits angiogenesis and tumor growth. *Blood* 102, 184–191.
- Yang, Y., Jun, C.D., Zhang, R., Joachimiak, A., Springer, T.A., and Wang, J.H. (2004). Structural basis for dimerization of ICAM-1 on the cell surface. *Mol. Cell Biochem.* 14, 269–276.
- Ye, Z., Zhang, C., Tu, T., Sun, M., Liu, D., Lu, D., Feng, J., Yang, D., Liu, F., and Yan, X. (2013). Wnt5a uses CD146 as a receptor to regulate cell motility and convergent extension. *Nat. Commun.* 4, 2803.
- Zhang, L., Luo, Y., Teng, X., Wu, Z., Li, M., Xu, D., Wang, Q., Wang, F., Feng, J., Zeng, X., et al. (2018). CD146: a potential therapeutic target for systemic sclerosis. *Protein Cell* 9, 1050–1054.
- Zheng, C., Qiu, Y., Zeng, Q., Zhang, Y., Lu, D., Yang, D., Feng, J., and Yan, X. (2009). Endothelial CD146 is required for in vitro tumor-induced angiogenesis: the role of a disulfide bond in signaling and dimerization. *Int. J. Biochem. Cell Biol.* 41, 2163–2172.
- Zhuang, J., Jiang, T., Lu, D., Luo, Y., Zheng, C., Feng, J., Yang, D., Chen, C., and Yan, X. (2010). NADPH oxidase 4 mediates reactive oxygen species induction of CD146 dimerization in VEGF signal transduction. *Free Radic. Biol. Med.* 49, 227–236.

iScience, Volume 24

Supplemental information

**Structure basis for AA98 inhibition
on the activation of endothelial cells
mediated by CD146**

Xuehui Chen, Huiwen Yan, Dan Liu, Qingji Xu, Hongxia Duan, Jing Feng, Xiyun Yan, and Can Xie

Supplemental Information

Structure Basis for AA98 Inhibition on the Activation of Endothelial Cells Mediated by CD146

Xuehui Chen, Huiwen Yan, Dan Liu, Qingji Xu, Hongxia Duan, Jing Feng, Xiyun Yan
and Can Xie

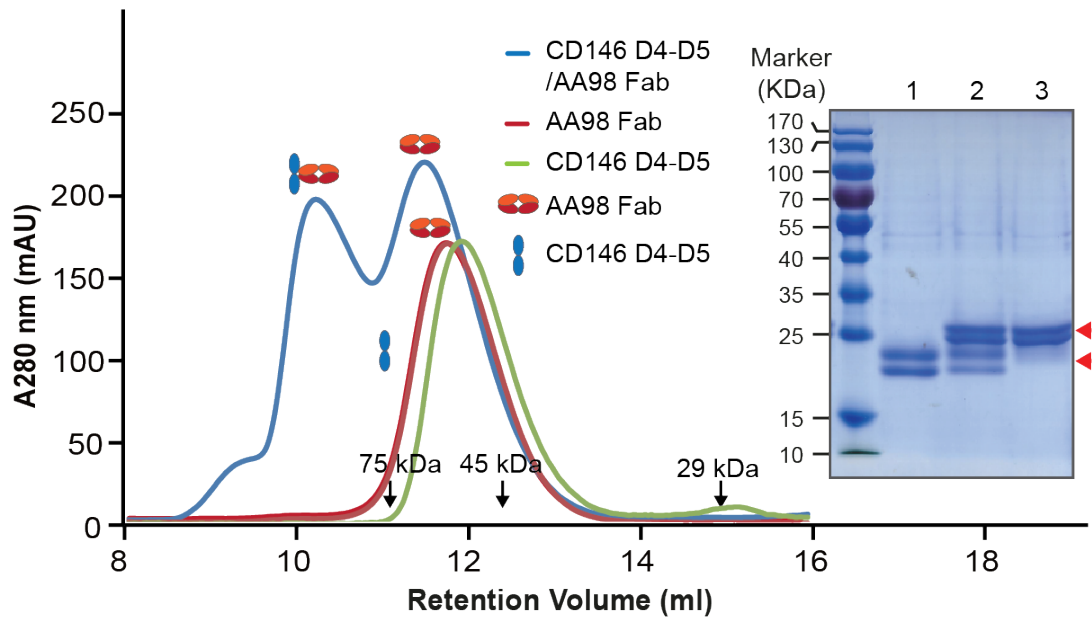


Figure S1. Protein purification of CD146 D4-D5 in complex with AA98 Fab. Related to Figure 1. Size-exclusion chromatography (Superdex 75 10/300 GL) analysis of purified CD146 D4-D5 protein (residues 336-519, green curve), AA98 Fab (red curve), and complex CD146 D4-D5/AA98 Fab protein (blue curve). SDS-PAGE (Inset) shows the purified CD146 D4-D5 from the peak of the green curve (Lane 1), the purified Fab AA98 from the peak of the red curve (Lane 3) and the complex CD146 D4-D5/AA98 Fab protein from the first peak of the blue curve (Lane 2). All eluted fractions were analyzed by 12% SDS-PAGE and stained with Coomassie Brilliant Blue. Black arrows indicate the elution positions for the standard marker in size-exclusion chromatography and red arrows show the position of CD146 D4-D5 protein and AA98 Fab in SDS-PAGE.

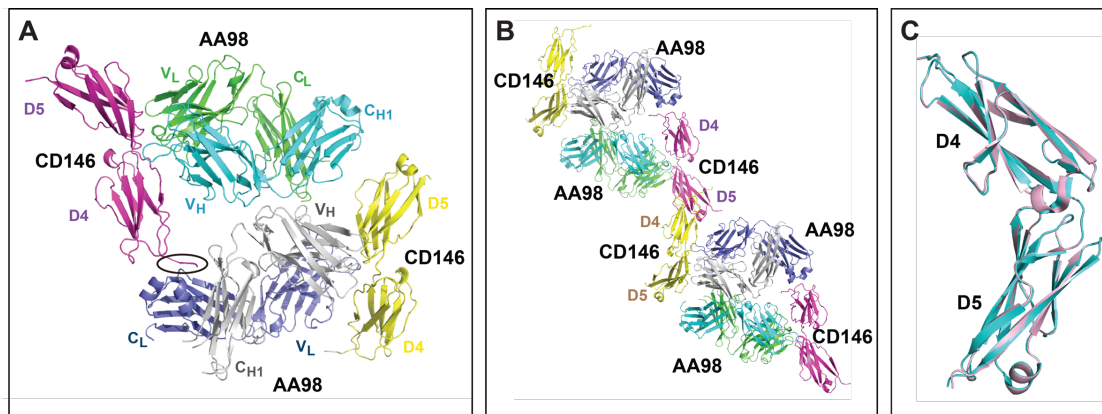


Figure S2. Crystal structure of CD146 D4-D5/AA98 Fab complex in the asymmetric unit. Related to Figure 1. (A) Two CD146 D4-D5/AA98 Fab complexes in the asymmetric unit. **(B)** Ribbon diagram of CD146 D4-D5/AA98 Fab complexes from two adjacent asymmetric unit which have interactions in CD146 part due to crystal packing. In the asymmetric unit, major interactions between different complex are those from AA98 Fab molecules. Apart from this, the extended loop from the remnant of CD146 D3 and D3-D4 linker (residues 337-341, elliptical part in **A**) interacted with the κ chain of another AA98 Fab (as shown in **B**). This is also the same part which interacts with the bottom of D5 from another symmetry related CD146 molecule (as shown in **B**). **(C)** Superposition of CD146 D4-D5 in asymmetric unit. CD146 D4-D5 molecules from asymmetric unit were superposed. One molecule is colored in lightpink while the other in cyan. The r.m.s.d. from the superposition of the CD146 C α atoms are 0.31 Å. These two molecules are almost identical except for the tail of D5.

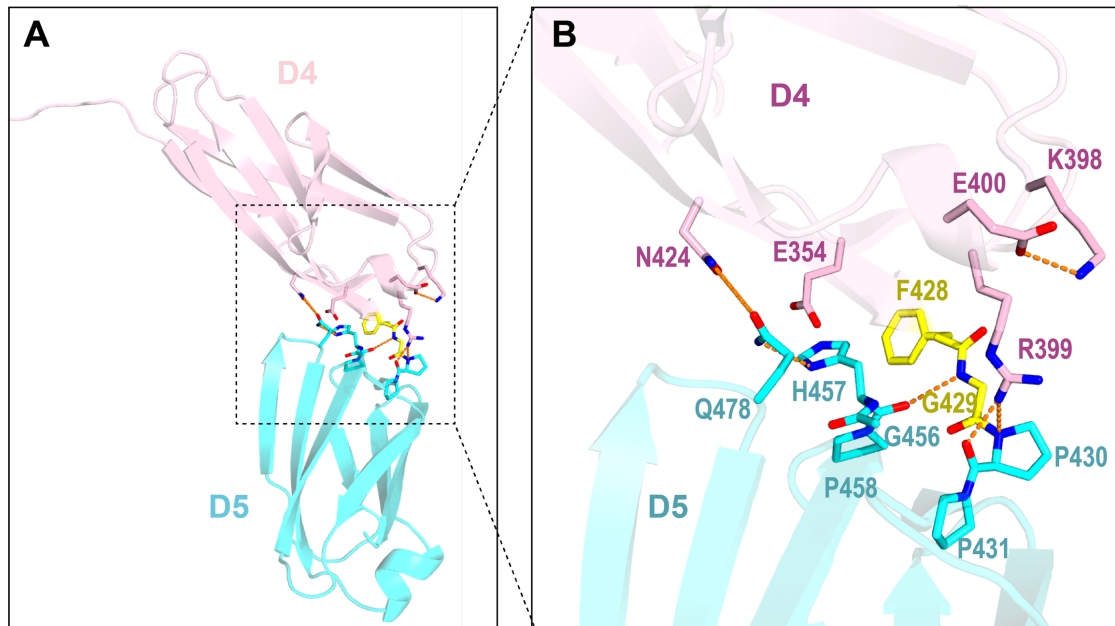


Figure S3. Interface between CD146 D4 and D5. Related to Figure 1. (A) Interface between CD146 D4 and D5 (AA98 Fab omitted for clarity). CD146 D4-D5 are shown in cartoon representation, and residues in D4 is colored in light pink, while those in D5 is colored in cyan. The two residues in the D4-D5 linker are colored in yellow. Residues in the D4-D5 interface are shown in sticks. (B) Enlargement of the residues in the red dashed line box, describing the direct interactions between D4 and D5 in the presence of AA98 Fab (omitted for clarity). Oxygen atoms are colored red and nitrogen atoms are blue. Hydrogen bonds are shown by orange dashed lines. For clarity, some residues and related interactions are omitted. Colors are as described in A.

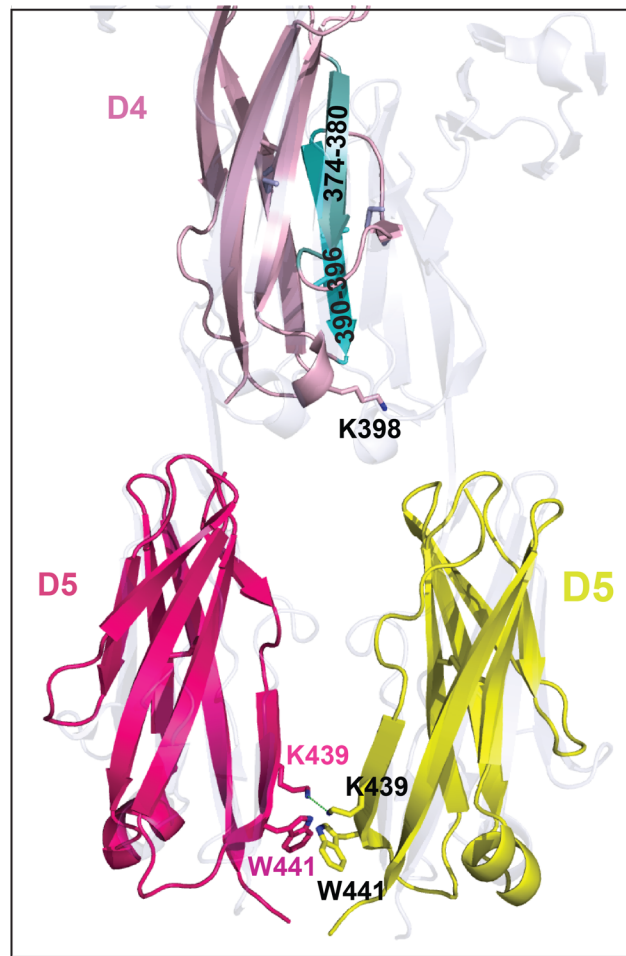


Figure S4. Identification of the potential CD146 dimer interface. Related to Figure 2. Superposition of CD146 D4-D5 on the corresponding domains of the ICAM-1 D3-D5 dimeric form. ICAM-1 D3-D5 is shown as the background and color in lightblue. One molecule of CD146 D4 is shown in lightpink and D5 in hotpink. Another CD146 D5 is superposed on the ICAM-1 dimer D5 and color in yellow. The deleted fragments are labelled. 374E-380E fragment is colored in lightteal while fragment 390P-396D is colored in cyan. The two residues, K398 in CD146 D4 and K439 in CD146 D5, that contribute to the dimerization in the chemical cross-linking test shown in stick representation. The dash line shows the distance between the two K439 from speculative adjacent CD146 D5. Also shown in stick representation are residues W441 in D5.

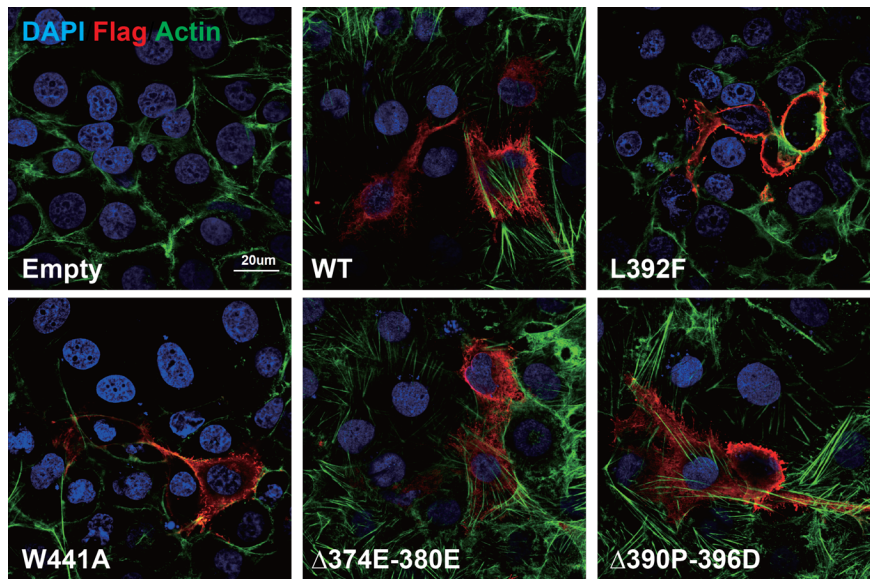


Figure S5. Decreased assembly of F-actin caused by CD146 steady-state. Related to Figure 3. Assembly of F-actin in HUVECS transfected with CD146 wild-type and CD146 mutants. Bar = 20 μ m.

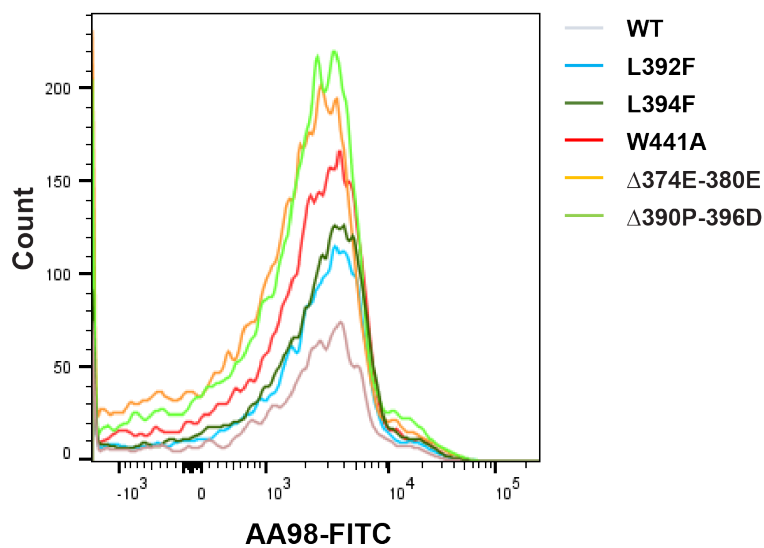


Figure S6. The mutations on CD146 do not affect AA98 binding. Related to Figure 3. 293T cells were transfected with constructs containing CD146 mutations, and AA98 binding affinity to different CD146 mutants were measured with FITC labeled AA98 mAb by FACS.

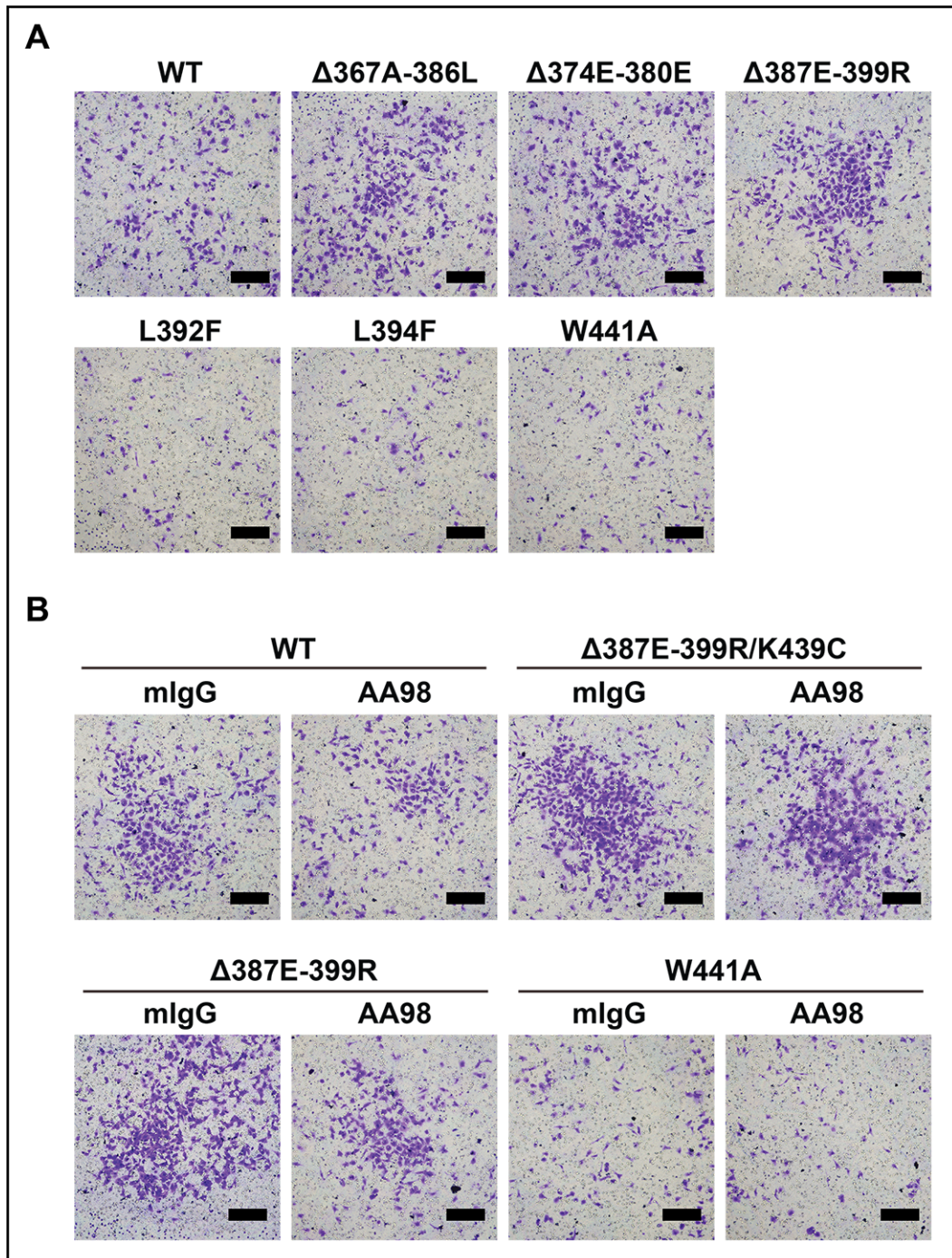


Figure S7. The representative images in the transwell migration assays. Related to Figure 3. (A) HUVECs transfected with different mutant constructs of CD146 were subjected to a transwell migration assay and representative images were shown (related to Figure 3C). **(B)** Transwell assay analysis of the migration activity of mutants transfected with HUVECs treated with AA98 or not and representative images were shown (related to Figure 3F). Bar = 50 μ m.

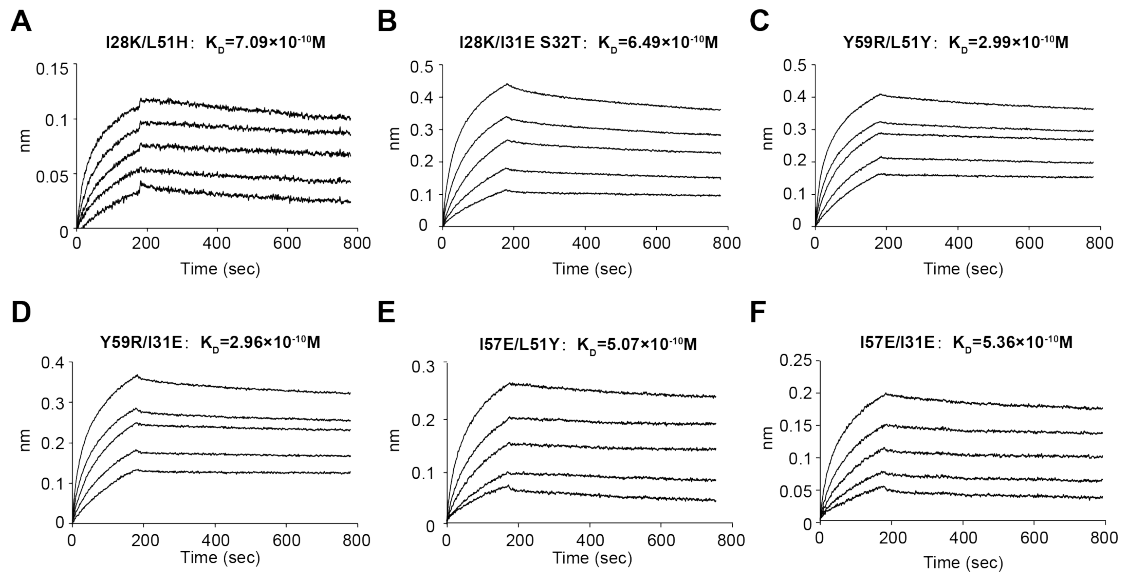


Figure S8. The improved binding affinity of rationally designed AA98 mutants to CD146. Related to Figure 4. BLI-binding assay was used to measure the affinity of a series of AA98 mutations, which were rationally designed to improve the binding affinity to CD146. A-F correspond to I28K/L51H, I28K/I31E, Y59R/L51Y, Y59R/I31E, I57E/L51Y, and I57E/I31E, respectively.

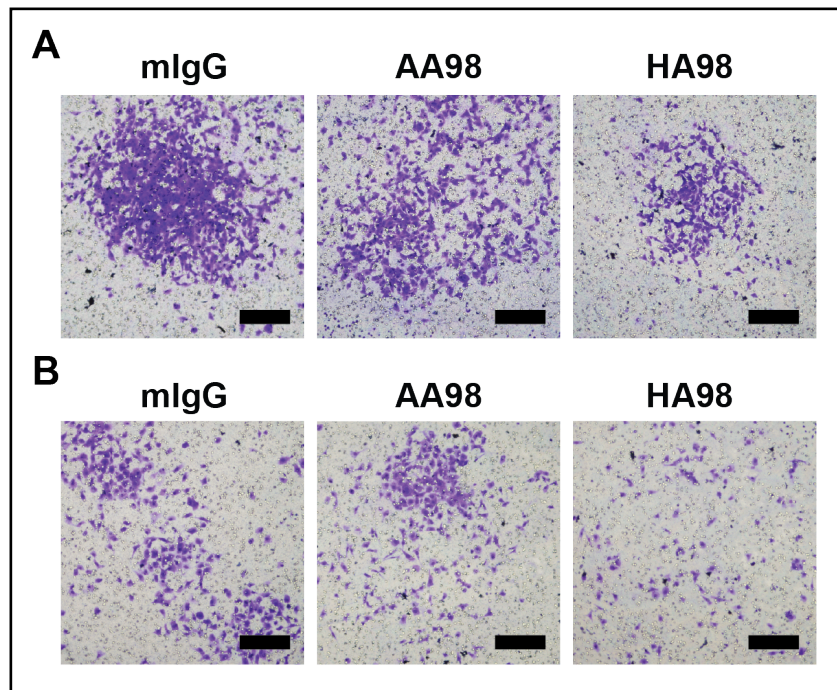


Figure S9. The representative images in the transwell migration assays. Related to Figure 4. MDA-MB-231 (A) and HUVECs (B) treated with mIgG (control), AA98 and HA98 were subjected to a transwell migration assay and representative images were shown, related to Figure 4F and Figure 4G, respectively. Bar = 50 μ m.

Transparent Methods

Recombinant Protein Expression and Purification

The construct for the CD146 domain 4-5 fragment (Gln336-Leu519) was inserted into the expression vector pEF1/puro (a vector based on pEF1/V5-HisA modified to contain a puromycin sequence). We added a CD146 signal peptide, followed by a His tag and an SBP tag, to the N-terminus of the fragment. A PreScission protease recognition sequence was introduced between the SBP tag and the CD146 D4-D5 fragment. Recombinant proteins were purified from CHO Lec 3.2.8.1 cell supernatants by affinity chromatography (Ni-NTA followed by strep-tactin column). The purified protein was digested with PreScission protease to remove the fused affinity tag and further deglycosylated with endoglycosidase H. Undigested proteins and protease were removed by reloading onto a Ni-NTA column. The CD146 D4-D5 protein was further purified by Superdex 200(GE Healthcare Life Sciences, Chalfont) gel filtration in 10 mM Tris-HCl, pH 8.0, 0.15 M NaCl.

The AA98 antibody was purified from the culture supernatant with a protein A column followed by Superdex 200 (GE Healthcare Life Sciences, Chalfont) gel filtration. The Fab was generated by immobilized papain (Pierce, Rockford, IL) digestion following the manufacturer's instructions. Undigested IgG and Fc fragments were removed by reloading onto the Protein A column, and the Fab was purified further by Superdex 75 (GE Healthcare Life Sciences, Chalfont) gel filtration in 20 mM HEPES, pH 7.5, 0.15 M NaCl. The purified CD146 D4-D5 fragment was incubated with AA98 Fab at a 1:4 molar ratio on ice for 30 min. The D4-D5 complex with Fab was separated from excess free Fab using Superdex 200 (GE Healthcare Life Sciences, Chalfont) in 10 mM Tris (pH 8.0) and 150 mM NaCl and

concentrated for crystallization.

Crystallization

Crystals were grown by using vapor diffusion in hanging drops at 291 K with equal volumes of 12 mg/ml protein solution and a reservoir solution of 19% PEG2000MME / 50 mM HEPES (pH 7.8). Crystals were cryoprotected by transfer to Ail's oil. The sequence of the AA98 Fab was determined by hybridoma cDNA sequencing exactly as previously described(Chen et al., 2007).

Structure Determination and Refinement

The diffraction data were collected at the 19-ID beamline of the Shanghai Synchrotron radiation Facility (SSRF, China)(Zhang et al., 2019) and processed with the program suite HKL2000(Otwinowski and Minor, 1997). The Phaser program(McCoy et al., 2007) was used for molecular replacement. The model used was the Fab fragment from D2.3 (PDB code1YEC(Charbonnier et al., 1997)). The solutions from molecular replacement were subjected to iterative cycles of model rebuilding in COOT(Emsley et al., 2010) and refinement using Phenix(Adams et al., 2010). After several cycles of refinement, manual model building and refinement for CD146 D4-D5 were performed. Sigma A-weighted 2 Fo-Fc and Fo-Fc maps were computed during the refinement, and refinement was monitored by the decrease in R_{free} . Composite omit maps were calculated during refinement to reduce model bias. The final model, refined to 2.8Å resolution, contains amino acid residues 336–519 of CD146 D4–D5, residues 1–217 of the AA98 Fab light chain, residues 1–132 and 138–217 of the Fab heavy chain, and two carbohydrate residues. Model geometry was verified using the program ProCheck(Laskowski et al., 1993). Solvent molecules were located from stereo

chemically reasonable peaks in the σ A-weighted Fo-Fc map. Final refinement statistics are summarized in Table 1. Structural figures were prepared with the program PyMol(DeLano, 2002).

Expression and Purification of AA98 Mutants

Gene sequences of AA98 mutants were cloned into the pEF expression vectors. Various variable regions were subcloned into expression vectors containing the appropriate mouse IgG2a H- and L-chain constant-region sequences by extension PCR. Constructs with different combinations of the light chain and the heavy chain were transiently cotransfected into 293T cells. The conditioned media from the transient production run were harvested and clarified by centrifugation. The supernatants were purified with a Protein A column as described above. Antibodies were further purified by size exclusion chromatography (Superdex 200 Increase 10/300 GL, GE Healthcare).

BLI-binding studies

Purified recombinant CD146 ectodomain was immobilized on Octet red system biosensors (Pall ForteBio, CA, USA). The bound CD146 ectodomain was diluted into kinetics buffer (PBS, pH 7.4, 0.01% (w/v) BSA, 0.002% (v/v) Tween-20) at 10 μ g/mL and immobilized onto AMC biosensors (FortéBio). Following a 120 s baseline step, biosensors were dipped into wells containing a two-fold dilution series of AA98 IgG. Sensors were then dipped back into kinetics buffer to monitor the dissociation rate. Kinetics data were analyzed using FortéBio's Data Analysis software 9.0, and kinetic curves were fitted to a 1:1 binding model. The mean kinetic constants reported are the results of three independent experiments.

Cell migration assay

Cell migration was assayed using a modified Boyden chamber assay (8 μm pore size; Costar; Corning) as described previously (Zheng et al., 2009). After the appropriate treatments, cells were trypsinized, washed, and resuspended in fresh serum-free medium (10,000 cells per well). After incubation at 37°C overnight, cells remaining at the upper surface of the membrane were removed using a swab, and cells that had migrated to the lower membrane surface, which are representative of migrated cells, were fixed with 4% paraformaldehyde and stained with Giemsa solution. Pictures were taken on an OLYMPUS BX51 microscope with a UPlanFLN digital camera using a 4/0.13 numeric aperture objective. Cells migrating through the filter were counted and plotted as the number of migrating cells per optic field.

Cell proliferation assay

The cell proliferation assay was conducted using the cell counting kit-8 (HY-K0301, MCE) following the manufacturer's instruction. Briefly, the cells were seeded into a 96-well plate in triplicates at the density of 3000 cells/100 μl . After 48 h, 10 μl dye solution was added and incubated at 37 °C for 3-4 h. The absorbance at 450 nm was measured using Mark microplate absorbance reader (Bio-Rad).

Immunofluorescence

Cells were plated on slides cultured in 6-well plates and then subjected to the appropriate treatments. The cells were washed with PBS, fixed in acetone/methanol (1:1) for 30 seconds, permeabilized with 0.1% Triton X-100, blocked with 5% normal goat serum for 60 min at 37°C, and then incubated with phalloidin for 1 hour. Coverslips were subsequently examined with a confocal laser scanning microscope (Olympus FLUOVIEW FV 1000) with an Olympus IX81 digital camera using a 20 \times /0.75 numeric aperture objective.

Immunohistochemistry

Paraffin-embedded tissue sections were deparaffinized and stained first with an antibody for CD31 and then with HRP-conjugated secondary antibody. The sections were then stained with 3,3'-diaminobenzidine(DAB) and finally counterstained with hematoxylin. The length of blood vessels per tumor in each group was quantified by ImagJ software in 10 random areas per section. Images were taken on a OLYMPUS BX51 microscope with a UPlanFL N digital camera using 10×/0.3 numeric aperture objective.

Animal experiments

Female 5-week-old BALB/c nude mice were kept under specific pathogen-free conditions. Xenografts of A375 cell lines were produced by injecting tumor cells (1×10^7 resuspended in PBS) subcutaneously into the backs of mice. When the tumors reached 5-8 mm, the mice were grouped (8 mice per group) and administered purified mAb HA98, AA98 or mIgG at a dose of 150 μ g per mouse twice per week by intraperitoneal injection. Tumor size was measured twice per week, and tumor volume was determined according to the following equation: tumor size = width² × length × (1/2).

This study was approved by the Ethical Review Committee of Institute of Biophysics, Chinese Academy of Sciences, China. All methods in this work were performed in accordance with the People's Republic of China regulation of experimental animals.

Statistical analysis

All experiments were done in triplicate. Data were shown as means \pm SEM. Statistical differences were determined by One-way ANOVA. $P < 0.05$ was considered statistically significant. The statistical analyses were performed with GraphPad Prism 5.0.

Data deposits

Atomic coordinates and the structure factor files have been deposited in the Protein Data Bank

(<http://www.rcsb.org>) under accession number 6LYN.

References

Adams P.D., Afonine P., Bunkóczi G, Chen V.B., Davis I.W., Echols N, Headd J.J, Hung L.W., Kapral G.J., Grosse-Kunstleve R.W. et al. (2010). PHENIX: a comprehensive Python-based system for macromolecular structure solution. *Acta Crystallogr D Biol Crystallogr.*, 66, 9. 10.1107/S0907444909052925

Charbonnier JB, Golinelli-Pimpaneau B., Gigant B, Tawfik DS, Chap R, Schindler DG, Kim SH, Green BS, Eshhar Z and Knossow M. (1997). Structural convergence in the active sites of a family of catalytic antibodies. *Science*, 275, 3. 10.1126/science.275.5303.1140

Chen, X., Kim, T. D., Carman, C. V., Mi, L. Z., Song, G. and Springer, T. A. (2007). Structural plasticity in Ig superfamily domain 4 of ICAM-1 mediates cell surface dimerization. *Proc Natl Acad Sci*, 104, 8. 10.1073/pnas.0707406104

DeLano, W. I. (2002). The PyMOL Molecular Graphics System, Version 2.0 Schrodinger, LLC.

Emsley, P., Lohkamp, B., Scott, W. G. and Cowtan, K. (2010). Features and development of Coot. *Acta Crystallogr D Biol Crystallogr*, 66, 486-501. 10.1107/S0907444910007493

Laskowski, R., MacArthur, M. W., Moss, D. S., and Thornton, J. M. (1993). PROCHECK: a program to check the stereochemical quality of protein structures. *J. Appl. Cryst*, 26, 283-291.

McCoy, A. J., Grosse-Kunstleve, R. W., Adams, P. D., Winn, M. D., Storoni, L. C. and Read, R. J. (2007). Phaser crystallographic software. *J Appl Crystallogr*, 40, 658-674. 10.1107/S0021889807021206

Otwinowski Z and Minor. W. (1997). Processing of X-ray diffraction data collected in oscillation mode. *Methods Enzymol.* , 276, 20. 10.1016/S0076-6879(97)76066-X

Zhang, W., Tang, JC., Wang, SS. et al. (2019). The protein complex crystallography beamline (BL19U1) at the Shanghai Synchrotron Radiation Facility. *Nucl Sci Tech*, 30. 10.1007/s41365-019-0683-2

Zheng C, Qiu. Y., Zeng Q, Zhang Y, Lu D, Yang D, Feng J and Yan X. (2009). Endothelial CD146 is required for in vitro tumor-induced angiogenesis: the role of a disulfide bond in signaling and dimerization. *Int J Biochem Cell Biol.*, 41, 10. 10.1016/j.biocel.2009.03.014